ACS APPLIED MATERIALS & INTERFACES

Research Article

www.acsami.org

Langmuir–Schaefer Films for Aligned Carbon Nanotubes Functionalized with a Conjugate Polymer and Photoelectrochemical Response Enhancement

Vito Sgobba,[†] Gabriele Giancane,[‡] Donato Cannoletta,[§] Alessandra Operamolla,[⊥] Omar Hassan Omar,[∥] Gianluca M. Farinola,[⊥,∥] Dirk M. Guldi,[†] and Ludovico Valli*[,#]

[†]Department of Chemistry and Pharmacy, Friedrich-Alexander University, Egerlandstrasse 3 D-91058 Erlangen, Germany

[‡]Dipartimento Beni Culturali, Università del Salento, via D. Birago 64, 73100 Lecce, Italy

[§]Dipartimento di Ingegneria dell'Innovazione, Università del Salento, Via per Monteroni, 73100 Lecce, Italy

[⊥]Dipartimento di Chimica, Università degli Studi di Bari Aldo Moro, via Orabona 4, I-70126 Bari, Italy

[∥]Consiglio Nazionale delle Ricerche-Istituto di Chimica dei Composti Organometallici Bari (CNR-ICCOM-Bari), via Orabona 4, I-70126 Bari, Italy

[#]Dipartimento di Scienze e Tecnologie Biologiche ed Ambientali, Università del Salento, via per Monteroni, 73100 Lecce, Italy

Supporting Information

ABSTRACT: Single-walled carbon nanotubes (SWCNTs) were suspended in 1,2-dichloroethane by noncovalent functionalization with a low-band-gap conjugated polymer **1** alternating dialkoxyphenylene–bisthiophene units with benzo-[*c*][2,1,3]thiadiazole monomeric units. The suspended **1**/SWCNT blend was transferred onto different solid substrates by the Langmuir–Schaefer deposition method, resulting in films with a high percentage of aligned nanotubes. Photoelectrochemical characterization of **1**/SWCNT thin films on indium–tin oxide showed the benefits of SWCNT alignment for photoconversion efficiency.

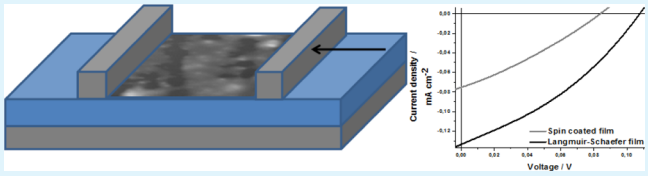

KEYWORDS: *Langmuir–Schaefer deposition, photoelectrochemical cell, optoelectronic, thin films, carbon nanotubes, conjugate polymers*

INTRODUCTION

Organic semiconductors are used as active materials in several optoelectronic devices including organic-based solar cells/photodetectors, field-effect transistors, and light-emitting diodes. Charge-transfer and charge-transport phenomena in solid thin films are strongly influenced by molecular arrangement[1,2] and intermolecular interactions.[3−5] Control over the supramolecular organization can lead to the formation of ordered films, where exciton dissociation and charge percolation are optimized.[6] In the last years, there has been special attention paid towards materials able to form optimized channels through the organic semiconducting matrix, where charges can be transported with low recombination probability.[7] As a leading example, carbon nanotubes are ideal candidates for charge transport in optoelectronic devices. Furthermore, these materials promptly accept or donate electrons when combined with electron donors[8,9] or with electron acceptors, respectively.[10]

A common issue related with carbon nanotubes wet processing is their limited suspendability in polar and nonpolar solvents. Strong van der Waals interactions between individual carbon nanotubes induce aggregate formation,[11,12] which renders them highly insoluble and nonprocessable for device applications. A largely pursued method to make single-walled carbon nanotubes (SWCNTs) suspendable is to covalently functionalize them with electrostatically charged substituents able to prevent their aggregation in bundled domains.[13] This approach induces strong modifications in the chemical structure of the carbon nanotube honeycomb, compromising their π-electronic network. An alternative approach that does not perturb the electronic structure of SWCNTs is based on noncovalent functionalization by van der Waals and $\pi-\pi$ interactions between carbon nanotubes and other conjugated materials. As an example, conjugated polymers strongly interact with SWCNTs by wrapping either ropes or individual tubes.[14,15] In the present work, a low-band-gap conjugated copolymer **1** containing thienylene, alkoxy-substituted phenylene, and benzothiadiazole units (Figure 1), previously synthesized as a donor material for bulk heterojunction solar cells,[16] was used to suspend the SWCNTs.

The deposition technique used for transferring noncovalently functionalized SWCNT suspensions onto solid substrates plays a crucial role in the molecular arrangement of the deposited film. Here, the Langmuir–Schaefer thin-film deposition

Received: August 30, 2013
Accepted: December 11, 2013
Published: December 11, 2013

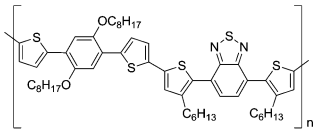

1

Figure 1. Chemical structure of polymer **1** used to suspend the SWCNTs.

method has been explored because it allows accurate control of both molecular packing and bidimensional orientation of the nanostructures.[14,17,18] This method has been reported in the literature for the deposition of thin films for applications in organic electronics (e.g., sensors[19] and transistors[20] as well as for biotechnological devices).[21]

MATERIALS AND METHODS

The SWCNTs (batch number: R 0510 C from Carbon Nanotechnologies Inc., with a purity of over 99%) used in this work were synthesized by disproportionation of carbon monoxide at high pressure and were not further purified. All solvents and indium–tin oxide (ITO) glasses were purchased from Sigma Aldrich (surface resistivity 8–12 Ω/sq).

The SWCNT suspension was obtained according to an already reported procedure[15] with slight variations: 1 mg of **1** was dissolved in 20 mL of 1,2-dichloroethane (DCE), and 1 mg of SWCNTs was added. The suspension was sonicated for 15 min at a temperature of 40 °C and centrifuged at 1600 rpm for 10 min. The liquid supernatant was collected and spread at the air/water interface of the Langmuir trough by using a glass syringe.

Polarization–modulation infrared reflection–absorption spectroscopy (PM-IRRAS) at the air/water subphase was carried out with a KSV instrument. During the experiments, after each run, the trough was carefully washed with chloroform, acetone, ethanol, and water. Ultrapure water (Millipore Milli-Q, 18.2 MΩ cm) was used as the subphase. Langmuir isotherm and Langmuir–Schaefer depositions were carried out in a KSV 5000 System 3 LB apparatus (850 cm^2). The barrier speed was fixed at 10 mm min^{-1} and the surface pressure was monitored using a Wilhelmy balance.

UV/vis measurements were carried out using a Perkin-Elmer Lambda 650 spectrometer, and Raman spectra were acquired with a Bruker FT-Raman RFS 100/S spectrometer with a YAG:Nd laser excitation source at 1064 nm.

Transmission electron microscopy (TEM) images were recorded with a Philips CM 300 UT high-resolution instrument (300 kV acceleration voltage, 0.172 nm point resolution; Scherzer focus) equipped with a two-camera system (TV System and CCD camera). Samples for TEM were prepared by casting 1 drop of the **1**/SWCNT sample suspension onto a standard Formvar film on a copper grid (230 meshes).

For photoelectrochemical characterization, ITO/(**1**/SWCNT)$_x$/I^-,I^-_3/Pt-FTO photoelectrochemical cells were constructed, modifying a previously reported procedure.[22] To prepare the counter electrode, a platinum catalyst was deposited on the FTO glass by coating with 1 drop of a 0.35 mM H_2PtCl_6 solution (2 mg of platinum in 1 mL of ethanol) and heating at 400 °C for 15 min. The electrolyte employed was a solution of 0.5 M LiI and 0.01 M I_2 in acetonitrile. For photocurrent measurements, a Keithley 2400 multimeter and a collimated light beam from a 350 W xenon lamp with a AM 1.5 filter were utilized. The light intensity for white-light measurements was 100 mW cm^{-2}. When a photoaction spectrum was recorded, a monochromator was introduced into the path of the excitation beam to select the required wavelengths: from 350 to 690 nm, 20 nm step. The EQE, defined as the number of electrons collected per incident photon, was evaluated from short-circuit photocurrent measurements at different wavelengths. The incident-light intensity was calibrated using a radiant-power/energy meter (Coherent Deutschland GmbH model Fieldmax II) before each experiment. All measurements were performed at 25 °C.

RESULTS AND DISCUSSION

Air/Water Interface Characterization. UV/vis/near-IR absorption spectra of **1** and **1**/SWCNT in DCE were first recorded to evaluate the interaction between host (**1**) and guest (SWCNT) (Figure 2). In the spectrum of **1**, two different

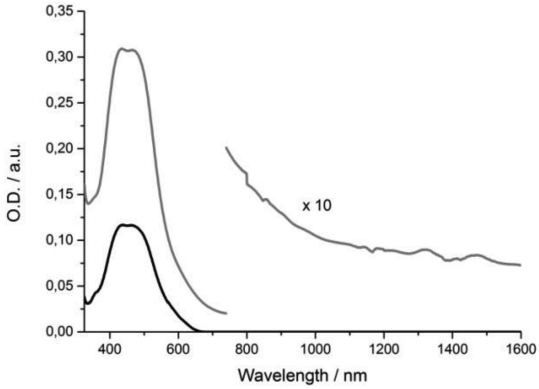

Figure 2. UV/vis/near-IR spectra of **1** (black line) and **1**/SWCNT (gray line) suspended in DCE.

absorption bands located at 437 and 463 nm are clearly observable. These peaks were respectively ascribed to the π–π^* electronic transition located on the thiophene-based segment and to the internal charge transfer between octyloxyphenylthiophene-based units and the benzothiadiazole moiety.[16] Looking at the **1**/SWCNT spectrum, several bands beyond 600 nm are observed and ascribed to the SWCNT van Hove singularities.

An aliquot of 150 μL of **1** dissolved in DCE at a concentration of 0.1 mg mL^{-1} was spread on the surface of an ultrapure water subphase, and the Langmuir isotherm was recorded during the barrier motion with a constant speed of 10 mm min^{-1} (Figure 3, gray line). A long pseudogaseous phase of **1**, indicating small interactions between the molecules spread on the subphase, is followed by a slope variation at about 100 $Å^2$/repeat unit with a limiting area per repeating unit of about

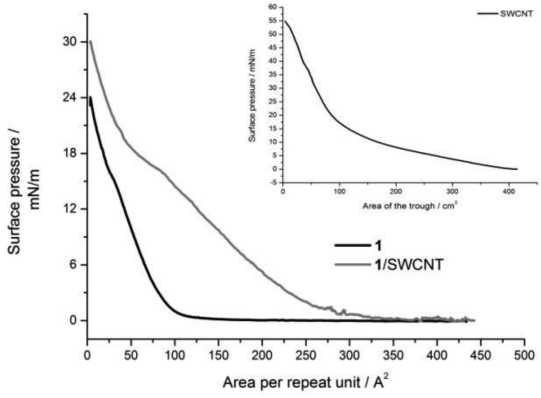

Figure 3. Langmuir isotherms of **1** (black line) and **1**/SWCNT (gray line) obtained by spreading 150 μL of a DCE solution. In the inset, the Langmuir isotherm of 150 μL of SWCNTs suspended in DCE is reported. Here, the *x* axis was reported as the area between the two Teflon barriers.

dx.doi.org/10.1021/am403656k | ACS Appl. Mater. Interfaces 2014, 6, 153–158

88 Å^2. When the same volume of **1**/SWCNT is spread at the air/water interface, an obvious reduction of the gaseous phase is recorded and a smoothed knee can be observed at about 250 Å^2. A further and sudden slope change at 16 mN/m suggests reorganization of the molecules constituting the floating layer. The two curves do not appear simply shifted, and the **1**/SWCNT pattern is not a linear combination of the isotherm of **1** and the Langmuir curve of the SWCNT suspension.[23] On the contrary, their trends appear deeply different, suggesting strong interactions between **1** and SWCNT.[24]

For closer investigation of the behavior of the spread materials at the interface, PM-IRRAS has been pursued. This spectroscopic technique is a powerful tool for the identification of the spatial arrangement of functional groups at the air/liquid interface. If the orientation of a molecular transition moment is parallel to the surface plane, the PM-IRRAS signal is equal to zero. On the contrary, if the orientation is perpendicular to the surface plane, the signal is maximum.[25] Parts a and b of Figure 4 show the IR spectra of **1** and the **1**/SWCNT Langmuir layer of the floating film recorded at the air/water interface at different surface pressures. Considering the spectrum of **1**, by increasing the surface pressure from 0.5 to 25 mN m^{-1} (Figure 4a), the strong bands at 991 and 1014 cm^{-1} ascribed to the vinyl rotation in the 1,4-arylene-2,5-thienylene moiety[26] and to the phenyl ether stretch vibrations, respectively, decrease. Notably, when the surface pressure increases from 0.5 to 7 mN m^{-1}, these two peaks are red-shifted from 1014 to 1032 cm^{-1} and from 991 to 995 cm^{-1}, respectively, owing to the forced aggregation of the polymer. The opposite trend is observed for the peak at 1091 cm^{-1} ascribed to the alkoxy group because, with an increasing in the surface pressure, the signal increases. Taking the aforementioned in concert, is safe to assume, with an increase in the surface pressure, phenylene and thiophene rings are tilting from the vertical to horizontal position and the alkyl chains are twisting vertically directed toward the air phase (Figure 4c).

On the contrary, in **1**/SWCNT PM-IRRAS spectra, the signal intensity does not significantly change during compression. This evidence is compatible with a scenario, where the polymer wraps up the SWCNTs and therefore does not change the configuration upon floating layer compression, similarly to what was reported in our previous study (see Figure 4b).[15]

Langmuir–Schaefer Film Characterization. Langmuir films of **1** were transferred on solid supports by means of the Langmuir–Schaefer deposition method at a surface pressure of 13 mN m^{-1}, which corresponds to the maximum packing of the polymer that is likely to be achievable on the air/water interface. **1**/SWCNT composite films were transferred at a surface pressure of 12 mN m^{-1}. Absorption spectra with polarized light were recorded to evaluate a possible organized arrangement of the species transferred on the quartz slides.[27] The two absorption bands ascribed to the polymer are red-shifted by about 30 nm in comparison with the absorption spectra recorded for the suspension in Figure 2, owing to aggregation in the film.[28] Visible spectra of **1** films obtained after 15 runs recorded with perpendicular and parallel incident light show a dichroic ratio at 530 nm of 1.12 that indicates an approximately random arrangement of deposited molecules (Figure 5a). In contrast, for **1**/SWCNT films obtained after 15 deposition runs, the absorption peak at 530 nm when light is polarized parallel to the barriers is 1.71 times more intense than the absorption recorded by shedding light polarized perpendicular to the barriers. These findings suggest an enhanced

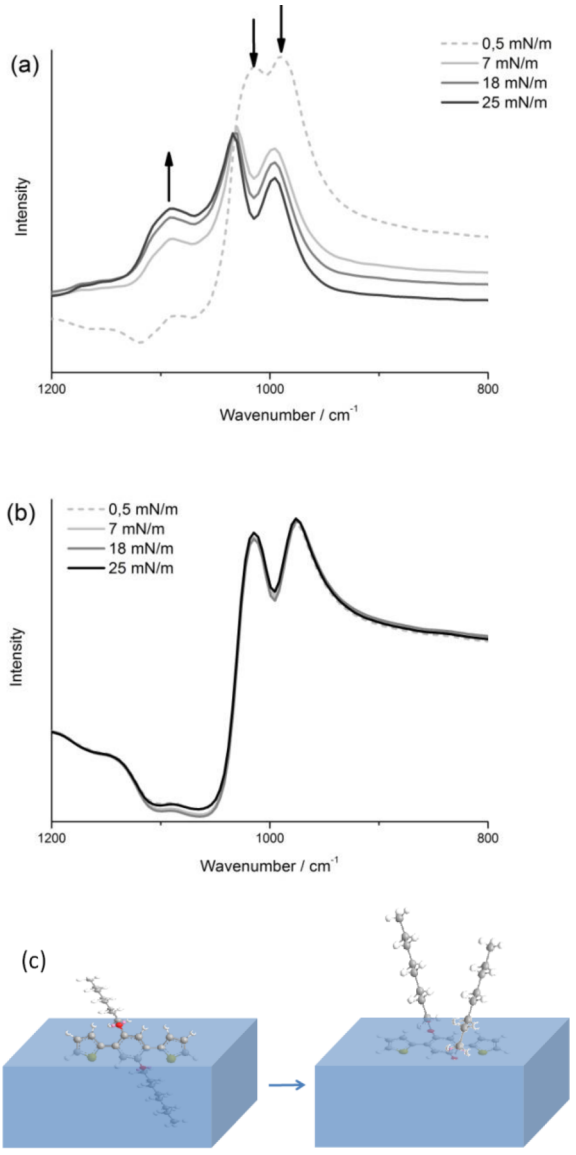

Figure 4. PM-IRRAS of (a) **1** and (b) **1**/SWCNT floating films at different surface pressures. (c) Schematic representation of the conformational changes in the 1,4-arylene-2,5-thienylene moiety of the polymer backbone at the surface of the water with an increase in the surface pressure.

alignment percentage yield of SWCNT in the **1**/SWCNT deposited film and strong supramolecular interactions between the polymer and nanotubes, in agreement with IRRAS analysis. In the range between 900 and 1500 nm, bands related uniquely to carbon nanotubes are discernible. The spectra obtained with polarized light in Figure 5b evidence a preferential arrangement of deposited SWCNT, as a function of the deposition direction. As a control experiment, the **1**/SWCNT was transferred by means of a spin-coating method, and films revealed a dichroic ratio of about 1:1, corroborating the effectiveness of the Langmuir–Schaefer deposition method in controlling the SWCNT orientation in the solid film.

Similar conclusions emerge from Raman spectroscopic analysis (Figure 6). The G band (at 1590 cm^{-1}), D band (1277 cm^{-1}), and radial breath mode bands (at ca. 300 cm^{-1}) are more intense when laser polarization parallel to the deposition direction is used. Again, the preferential orientation

dx.doi.org/10.1021/am403656k | ACS Appl. Mater. Interfaces 2014, 6, 153–158

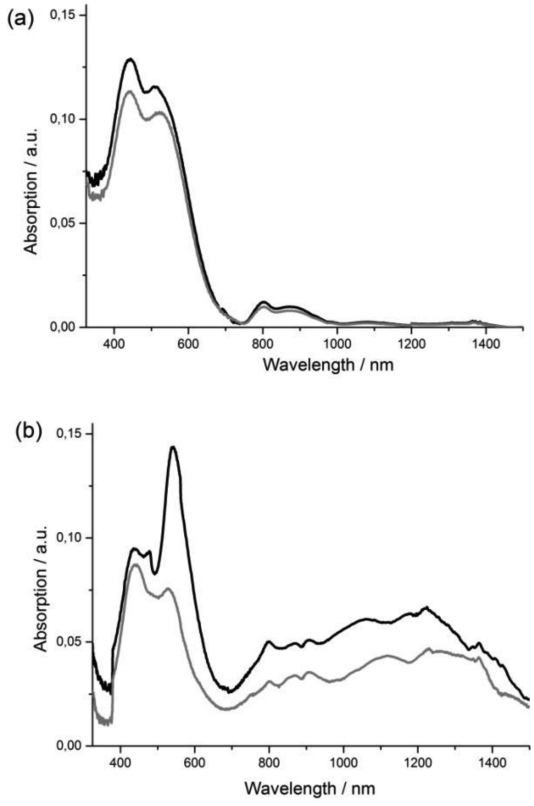

Figure 5. Absorption spectra of 15 Langmuir–Schaefer layered films of (a) **1** and (b) **1**/SWCNT upon illumination with parallel (black line) and perpendicular (gray line) polarized incident light.

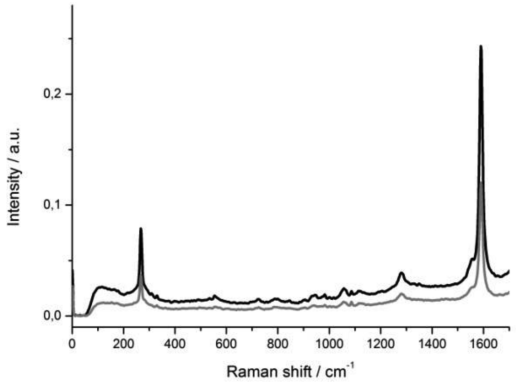

Figure 6. Raman spectra (excitation at 1064 nm) of a **1**/SWCNT Langmuir–Schaefer film (10 deposition runs) upon illumination with parallel (black line) and perpendicular (gray line) polarized incident light.

of **1**/SWCNT in the transferred film induced by the Langmuir–Schaefer deposition method is evident.

Atomic force microscopy (AFM) images show large interwoven $(\mathbf{1}/\mathrm{SWCNT})_x$ aggregates with diameter up to micrometer size and prevalently oriented along the *y* direction, as shown in Figure 7.

TEM characterization of the film cast from the **1**/SWCNT suspension suggests that polymer **1** envelopes small bundles of SWCNTs (Figure 8), as previously supposed from the PM-IRRAS results at the air/water interface.

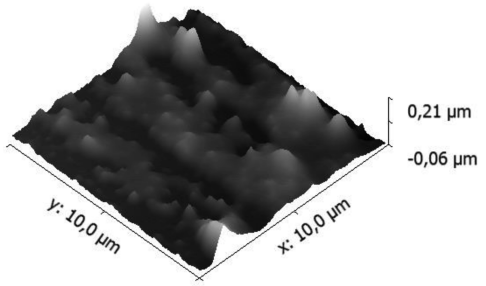

Figure 7. AFM 3D image of a ITO/$(\mathbf{1}/\mathrm{SWCNT})_{50}$ Langmuir–Schaefer film.

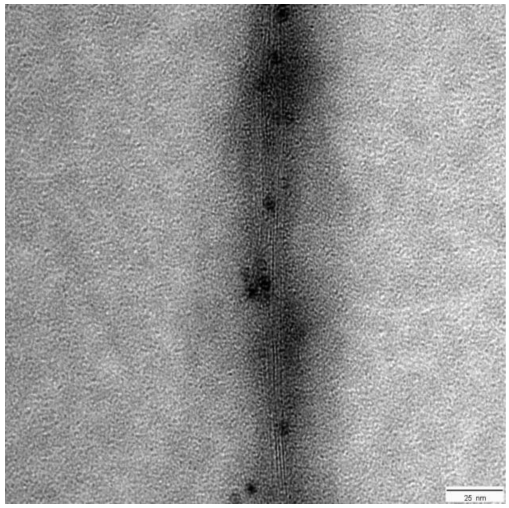

Figure 8. TEM image of a **1**/SWCNT film obtained by casting a drop of its suspension in DCE. The scale bar is 25 nm.

X-ray diffractometry of the **1**/SWNTs Langmuir–Schaefer film showed weak (002) and (100) peaks at 2θ of 26.8° and 42.8°, respectively. The (002) peak arises from contact points between neighboring SWNTs, whereas the (100) peak originates from the graphitic structure. When turning on the SWNTs/**1** cast films, owing to their disordered morphology, these peaks are not ascernible (see Figure S1 in the Supporting Information).

Photoelectrochemical Characterization of a 1/SWCNT Langmuir–Schaefer Film. To quantify the benefit of probed supramolecular organization on charge transfer and charge transport for solar light conversion, we constructed ITO/$(\mathbf{1}/\mathrm{SWCNT})_{10}/\mathrm{I}^-,\mathrm{I}^-_3$/Pt-FTO photoelectrochemical cells, where **1**/SWCNT photoactive films were deposited by Langmuir–Schaefer and spin-coating techniques provided that they bear the same light-harvesting efficiency.

From the current–voltage characteristics, owing to the p-type nature of both **1**[15] and SWCNT,[9] a photocathodic current is observed. The two cells revealed different open-circuit voltages (V_{oc}, 0.11 and 0.084 V) and short-circuit currents (J_{sc}). J_{sc} observed from the cell, where the **1**/SWCNT film is deposited by the Langmuir–Schaefer method (−0.133 mA cm^{-2}) is almost double compared with the J_{sc} of the cell, where the **1**/SWCNT film was obtained by spin coating (−0.07 mA cm^{-2}); see Figure 9. Because light harvesting for the two cells was the same, the photocurrent enhancement in devices bearing Langmuir–Schaefer films originated from improved internal quantum efficiency, namely the efficiency with which

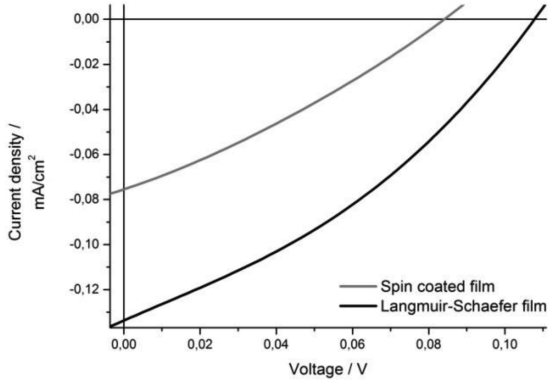

Figure 9. $J-V$ characteristics of ITO/(**1**/SWCNT)$_x$/I^-,I^-_3/Pt-FTO photoelectrochemical cells, where **1**/SWCNT was deposited by the Langmuir–Schaefer method (10 deposition runs) (black line) and by spin coating (gray line) under AM 1.5 illumination.

absorbed photons generate collectable carriers, in the **1**/SWCNT 3D network.

To enhance the light harvesting, thicker multistack films were constructed, and photoaction spectra were recorded (Figure 10b). These show two maxima at around 450 and 540 nm.

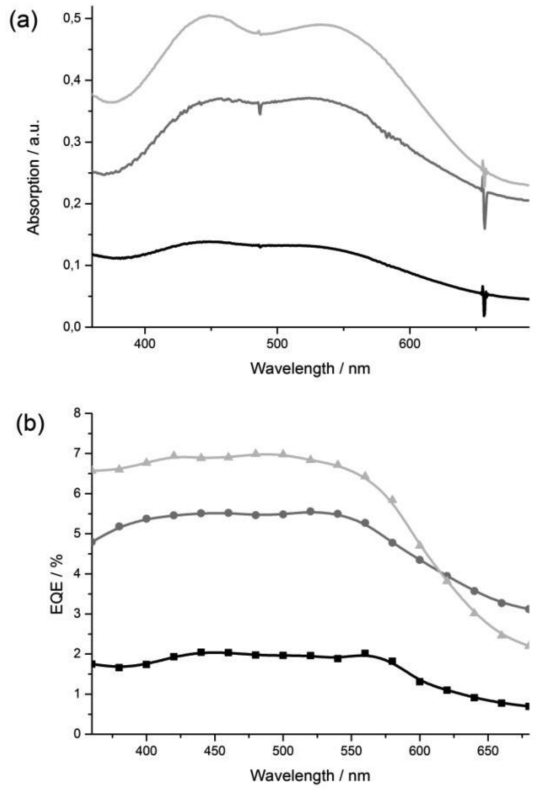

Figure 10. (a) Absorption and (b) photoaction spectra of ITO/(**1**/SWCNT)$_n$/I^-,I^-_3/Pt-FTO with n = 50 (black line), 80 (gray line), and 96 (light-gray line) deposition runs.

Their resemblance to the absorption maxima of the **1**/SWCNT film on ITO (Figure 10a) indicates that the predominantly active component is **1**. The good agreement between absorption and photoaction spectra shows that **1** is the main light-absorbing material. Thus, light is initially absorbed by **1** throughout the different layers, followed by rapid electron transfer from **1** to SWCNT and from SWCNT to the electrolyte. The neutrality of **1** is restored by electron transfer from the ITO electrode, while the electrolyte is reoxidized at the platinum counter electrode.

For the optimized film obtained upon 96 Langmuir–Schaefer runs, the $J-V$ characteristic revealed J_{sc} of 0.7 mA cm^{-2}, V_{oc} of 0.12 V, a fill factor of 30%, and a maximum power energy efficiency of 29.9 × 10^{-3}% (Figure 11). Thicker films revealed lower performances owing to the larger series resistance of the multistack that overcompensates for the benefit of enhanced light harvesting.

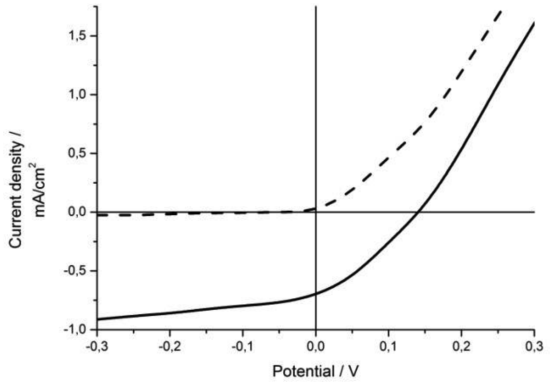

Figure 11. $J-V$ characteristics of ITO/(**1**/SWCNT)$_x$/I^-,I^-_3/Pt-FTO photoelectrochemical cells, where **1**/SWCNT was deposited by the Langmuir–Schaefer method (96 deposition runs) in the dark (dashed line) and under AM 1.5 illumination (solid line).

CONCLUSIONS

A suspension of SWCNT in DCE was obtained by means of noncovalent functionalization by synthetic polymer **1** that wraps up bundles of a few nanotubes, breaking the strong van der Waals interactions between SWCNTs. This procedure allows the formation of a very stable suspension of **1**/SWCNT that was spread at the air/water interface in a Langmuir through. The floating film has been transferred on different solid substrates, and spectroscopic measurements with polarized light suggest the formation of a highly oriented thin film. TEM pictures confirm the hypothesis that **1** wraps up the SWCNTs. Photoelectrochemical cells based on ITO/(**1**/SWCNT)$_x$ photoelectrodes obtained by the Langmuir–Schaefer technique exhibit significantly improved device performances, specifically, 47% enhanced photocurrent, relative to cells that are fabricated by spin coating. The difference in the photoresponse confirms the benefits of the molecular order induced by the Langmuir–Schaefer deposition method. We believe that the present results suggest a potent alternative for fabricating photoactive molecular devices.

ASSOCIATED CONTENT

Supporting Information

XRD diffractogram of (SWNTs/**1**)$_{10}$. This material is available free of charge via the Internet at http://pubs.acs.org.

AUTHOR INFORMATION

Corresponding Author

*E-mail: ludovico.valli@unisalento.it.

Notes

The authors declare no competing financial interest.

■ ACKNOWLEDGMENTS

This work was financially supported by Ministero dell'Istruzione, dell' Università e della Ricerca (MIUR), by Università degli Studi di Bari Aldo Moro, Progetto PRIN 2009 ["Innovative materials for organic and hybrid photovoltaics (prot. 2009PRAM8L)"], by Università del Salento [Progetto PRIN 2010-2011, ref 2010N3T9M4_003: nanostrutture gerarchiche fotosintetiche per la produzione di energia]; by Regione Puglia, Costituzione di Reti di Laboratori Pubblici di Ricerca, Progetto Esecutivo 09, WAFITECH, by PON Ricerca e Competitività (2007-2013, Prog. 2HE), by the Deutsche Forschungsgemeinschaft as part of the Excellence Cluster "Engineering of Advanced Materials", and by the Bayerische Staatsregierung as part of the "Solar Technologies go Hybrid" initiative.

■ REFERENCES

(1) Rand, B. P.; Cheyns, D.; Vasseur, K.; Giebink, N. C.; Mothy, S.; Yi, Y.; Coropceanu, V.; Beljonne, D.; Cornil, J.; Brédas, J. L.; Genoe, J. *Adv. Funct. Mater.* **2012**, *22*, 2987−2995.

(2) Olguin, M.; Zope, R. R.; Baruah, T. *J. Chem. Phys.* **2013**, *138*, 0743061−0743068.

(3) Beljonne, D.; Curutchet, C.; Scholes, G. D.; Silbey, R. J. *J. Phys. Chem. B* **2009**, *113*, 6583−6599.

(4) Rahman, G. M. A.; Guldi, D. M.; Cagnoli, R.; Mucci, A.; Schenetti, L.; Vaccari, L.; Prato, M. *J. Am. Chem. Soc.* **2005**, *127*, 10051−10057. Cioffi, C.; Campdelli, S.; Sooambar, C.; Marcaccio, M.; Marcolongo, G.; Meneghetti, M.; Paolucci, D.; Paolucci, F.; Ehli, C.; Rahman, G. M. A.; Sgobba, V.; Guldi, D. M.; Prato, M. *J. Am. Chem. Soc.* **2007**, *129*, 3938−3945.

(5) Sgobba, V.; Troeger, A.; Cagnoli, R.; Mateo-Alonso, A.; Prato, M.; Schenetti, L.; Guldi, D. M. *J. Mater. Chem.* **2009**, *19*, 4319−4324.

(6) Grimm, B.; Schornbaum, J.; Jasch, H.; Trukhina, O.; Wessendorf, F.; Hirsch, A.; Torres, T.; Guldi, D. M. *Proc. Natl. Acad. Sci. U.S.A.* **2012**, *109*, 15565−15571.

(7) Kimber, R. G. E.; Walker, A. B.; Schröder Turk, G. E.; Cleaver, D. J. *Phys. Chem. Chem. Phys.* **2010**, *12*, 844−851.

(8) Baskaran, D.; Mays, J. W.; Zhang, X. P.; Bratcher, M. S. *J. Am. Chem. Soc.* **2005**, *127*, 6916−6917.

(9) Sgobba, V.; Guldi, D. M. *Chem. Soc. Rev.* **2009**, *38*, 165−184. Guldi, D. M.; Rahman, G. N. A.; Ramey, J.; Marcaccio, M.; Paolucci, D.; Paolucci, F.; Qin, S.; Ford, W. T.; Balbinot, D.; Jux, N.; Tagmatarchis, N.; Prato, M. *Chem. Commun.* **2004**, 2034−2035.

(10) Troeger, A.; Ledendecker, M.; Margraf, J.; Sgobba, V.; Guldi, D. M.; Vieweg, B. F.; Spiecker, E.; Suraru, S. L.; Würthner, F. *Adv. Environ. Mater.* **2012**, *2*, 536−540.

(11) Campidelli, S.; Klumpp, C.; Bianco, A.; Guldi, D. M.; Prato, M. *J. Phys. Org. Chem.* **2006**, *19*, 531−539.

(12) Sgobba, V.; Rahman, G. M. A.; Guldi, D. M.; Campidelli, S.; Prato, M. *Adv. Mater.* **2006**, *18*, 2264−2269.

(13) Rahman, G. M. A.; Troeger, A.; Sgobba, V.; Guldi, D. M.; Jux, N.; Tchoul, M. N.; Ford, W. T.; Mateo-Alonso, A.; Prato, M. *Chem.—Eur. J.* **2008**, *14*, 8837−8846.

(14) Li, X.; Zhang, L.; Wang, X.; Shinoyama, I.; Sun, X.; Seo, W. S.; Daj, H. *J. Am. Chem. Soc.* **2007**, *129*, 4890−4891.

(15) Giancane, G.; Ruland, A.; Sgobba, V.; Valli, L.; Manno, D.; Serra, A.; Farinola, G. M.; Hassan Omar, O.; Guldi, D. M. *Adv. Funct. Mater.* **2010**, *20*, 2481−2488.

(16) Operamolla, A.; Colella, S.; Musio, R.; Loiudice, A.; Hassan Omar, O.; Melcarne, G.; Mazzeo, M.; Gigli, G.; Farinola, G. M.; Babudri, F. *Sol. Energy Mater. Sol. Cells* **2011**, *95*, 3490−3503.

(17) Tanese, M. C.; Farinola, G. M.; Pignataro, B.; Valli, L.; Giotta, L.; Conoci, S.; Lang, P.; Colangiuli, D.; Babudri, F.; Naso, F.; Sabbatini, L.; Zambonin, P. G.; Torsi, L. *Chem. Mater.* **2006**, *18*, 778−784.

(18) Ulman, A. *An Introduction of Ultrathin Organic Films from Langmuir−Blodgett to Self-Assembly*; Academic Press: New York, 1991; Vol. *XXIII*; p 127−129.

(19) Giancane, G.; Guascito, M. R.; Malitesta, C.; Mazzotta, E.; Picca, R. A.; Valli, L. *J. Porphyrins Phthalocyanines* **2009**, *13*, 1129−1139.

(20) Nguyen, C. A.; Wang, J.; Chen, L.; Mhaisalkar, S. G.; Lee, P. S. *Org. Electron.* **2009**, *10*, 145−151.

(21) Vittorino, E.; Giancane, G.; Bettini, S.; Valli, L.; Sortino, S. *J. Mater. Chem.* **2009**, *19*, 8253−8258.

(22) Ito, S.; Murakami, T. N.; Comte, P.; Liska, P.; Graetzel, C.; Nazeeruddin, M. K.; Graetzel, M. *Thin Solid Films* **2008**, *516*, 4613−4619.

(23) Giancane, G.; Bettini, S.; Valli, L. *Colloids Surf., A* **2010**, *354*, 81−90.

(24) Lodi, A.; Momicchioli, F.; Caselli, M.; Giancane, G.; Ponterini, G. *RSC Adv.* **2013**, *3*, 1468−1475.

(25) Elzin, T.; Bistac, S.; Brogly, M.; Schultz, J. *Macromol. Symp.* **2004**, *205*, 181−190.

(26) Louarn, G.; Mevellec, J. Y.; Buisson, J. P.; Lefrant, S.; Eckhardt, H. *Electron. Prop. Polym.* **1992**, *107*, 298−303.

(27) Conoci, S.; Guldi, D. M.; Nardis, S.; Paolesse, R.; Kordatos, K.; Prato, M.; Ricciardi, G.; Vicente, M. G. H.; Zilbermann, I.; Valli, L. *Chem.—Eur. J.* **2004**, *10*, 6523−6530.

(28) In the films, two minor peaks are discernible around 800 and 900 nm, whose origin is, however, unknown to us at the present stage.